CH-99-1-4

Large Eddy Simulations of Smoke Movement

Kevin B. McGrattan, Ph.D. **Howard R. Baum, Ph.D.** **Ronald G. Rehm, Ph.D.**

ABSTRACT

This paper describes a methodology for simulating the transport of smoke and hot gases in buildings. The approach is based on the use of efficient CFD techniques and high-performance computers to solve a form of the Navier-Stokes equations specialized to the smoke movement problem. The fire is prescribed in a manner consistent with a mixture fraction-based approach to combustion, but the combustion phenomena themselves are not simulated. The mixing and transport of smoke and hot gases are calculated directly from an approximate form of the Navier-Stokes equations. The computations are three-dimensional and time-dependent and are limited only by the spatial resolution of the underlying grid. Due to the efficiency of the algorithm, calculations employing over a million computational cells are routinely performed on workstations. Convective motion is resolved down to scales one-hundredth the size of the characteristic length of the enclosure. For residential rooms or hotel units, this corresponds to 3-5 centimeter resolution, and for industrial applications, 10-20 centimeters. Fire-related phenomena such as radiative heat transfer, flame spread, and sprinkler spray dynamics have been added to the model, enabling simulations of large-scale fire experiments. Examples of how the model is used in this regard are presented.

INTRODUCTION

Computational fluid dynamics (CFD) is starting to become more commonly used by the fire research community to study the transport of combustion products from fires. The advantage of these techniques over traditional lumped parameter models is that they provide much finer spatial and temporal resolution and allow for the study of more detailed physical phenomena such as sprinkler sprays and flame spread. The role of CFD in fire research is not necessarily to replace experimentation altogether but rather to serve as a tool for planning and analysis. Most large research projects these days have both an experimental and computational component. Computations can be performed before the experiments to aid in their design and afterward to analyze results and bring to light phenomena that may be difficult to capture with single-point measurements.

The fluid flow simulation techniques described in this paper emphasize high spatial and temporal resolution and have been designed specifically to address the fire problem. The finite-difference model is often referred to as a large eddy simulation (LES). The use of the term "large eddy simulation" refers to the idea that the convective fluid motion should be simulated at the finest length and time scales allowed by a given computational grid. Much effort has been devoted to making the numerical code efficient, and calculations involving more than one million computational cells are routinely performed on modestly priced workstations. The spatial and temporal resolution afforded by such dense grids is absolutely critical if such phenomena as flame spread and sprinkler spray interaction are to be realistically simulated. Time-averaging arguments employed by most other field models simply cannot be applied to the extremely complicated scenarios considered.

One particular example of the combined use of experiment and computation is a research project sponsored by the National Fire Protection Research Foundation with financial support from interested industrial sponsors. The objective of the project is to evaluate the interaction of sprinklers, draft curtains (sheets of steel or similar material hung from the ceiling of a large enclosure for the purpose of inhibiting smoke

Kevin B. McGrattan is a mathematician and **Howard R. Baum** and **Ronald G. Rehm** are Fellows at the National Institute for Standards and Technology, Gaithersburg, Md.

spread, which are often used to enhance the performance of fire vents), and fire vents in large facilities. At issue is to what extent and under what conditions the combination of sprinklers with vents and/or draft curtains enhances or diminishes the performance of the sprinkler system. Experiments are now being performed to answer many of the questions. To complement the experiments, the NIST Large Eddy Simulation Fire Model has been used to help design the large-scale experiments that were intended to assess the relative performance of the vents and draft curtains under a variety of rack storage configurations. The results of the experiments are being used to assess the accuracy of the model and to suggest improvements to the fire-specific submodels. This exercise has greatly increased confidence in the model, allowing it to be used to expand the test matrix beyond that of the actual experiments, which were limited due to cost considerations.

Details of many of the fire-specific submodels, such as sprinkler spray dynamics and flame spread, will not be discussed in the present paper but, rather, the basic hydrodynamic capability of the model. Suffice it to say that the fire and the sprinklers serve as source terms in the fundamental equations. The ability of the model to predict the transport of smoke and hot gases from a fire is of importance here. To quantitatively assess the performance of the model, the results of simulations have been compared with experiments. These experiments range from measurements of velocities and temperatures within an isolated fire plume to scenarios involving the burning of racked commodities, sprinkler sprays, roof vents, and draft curtains.

MATHEMATICAL MODEL

Consider a thermally expandable ideal gas driven by a prescribed heat source. The equations of motion governing the fluid flow are written in a form suitable for low mach number applications (Rehm and Baum 1978). Sometimes this form of the equations is referred to as "weakly compressible." The most important feature of these equations is that in the energy and state equations the spatially and temporally varying pressure is replaced by an average pressure, p_0, that depends only on time. This is done to filter out acoustic waves. The efficiency of the numerical solution of the equations is dramatically increased by this approximation.

In the equations to follow, all symbols have their usual fluid dynamical meaning: ρ is the density, $\mathbf{u}$ the velocity vector, ω the vorticity, p the pressure, $\mathbf{g}$ the gravity vector, c_p the constant-pressure specific heat, T the temperature, k the thermal conductivity, t the time, $\dot{q}$ the prescribed volumetric heat release, $\Re$ the gas constant equal to the difference of the specific heats $\Re = c_p - c_v$, and σ the standard stress tensor for compressible fluids.

$$\frac{\partial \rho}{\partial t} + \nabla \cdot \rho \mathbf{u} = 0 \tag{1}$$

$$\rho\left(\frac{\partial \mathbf{u}}{\partial t} + \frac{1}{2}\nabla|\mathbf{u}|^2 - \mathbf{u}\times\omega\right) + \nabla p - \rho g = \nabla \cdot \sigma \tag{2}$$

$$\rho c_p\left(\frac{\partial T}{\partial t} + \mathbf{u}\cdot\nabla T\right) - \frac{dp_0}{dt} = \dot{q} + \nabla\cdot k\nabla T \tag{3}$$

$$p_0(t) = \rho \Re T \tag{4}$$

The divergence of the flow $\nabla \cdot \mathbf{u}$ is a very important quantity in the analysis to follow, and it is readily found by combining Equations 1 and 3 and by using the equation of state 4.

$$p_0 \nabla\cdot\mathbf{u} + \frac{1}{\gamma}\frac{dp_0}{dt} = \frac{\gamma-1}{\gamma}(\dot{q} + \nabla\cdot k\nabla T) \tag{5}$$

where $\gamma = c_p/c_v$. Integrating Equation 5 over the entire domain Ω yields a consistency condition for the background pressure $p_0(t)$.

$$p_0\int_{\partial\Omega} u\cdot dS + \frac{V}{\gamma}\frac{dp_0}{dt} = \frac{\gamma-1}{\gamma}\left(\int_\Omega \dot{q}\, dV + \int_{\partial\Omega} k\nabla T\cdot dS\right) \tag{6}$$

where V is the volume of the enclosure. The background pressure can be expressed in terms of a background temperature $T_0(t)$ and density $\rho_0(t)$.

$$p_0 = \Re \rho_0 T_0 \tag{7}$$

These spatially averaged quantities play the same role that ambient conditions do in the Boussinesq approximation. Perturbations to each are represented by the relations

$$T = T_0(t)(1+\tilde{T}) \quad ; \quad \rho = \rho_0(t)(1+\tilde{\rho}). \tag{8}$$

The perturbation values are thus simply related.

$$(1+\tilde{T})(1+\tilde{\rho}) = 1 \tag{9}$$

Defining T_0 and ρ_0 through the adiabatic process,

$$\frac{\rho_0}{\rho_\infty} = \left(\frac{p_0}{p_\infty}\right)^{1/\gamma}, \tag{10}$$

allows the energy equation to be expressed in terms of the perturbation temperature $\tilde{T}$ and the divergence.

$$\frac{\partial \tilde{T}}{\partial t} + u\cdot\nabla\tilde{T} = (1+\tilde{T})\left[\nabla\cdot u + \frac{1}{\gamma p_0}\frac{dp_0}{dt}\right] \tag{11}$$

The background pressure is found from Equation 6.

In the momentum equation, the pressure is composed of three components, the background $p_0(t)$, the hydrostatic, and a perturbation to the hydrostatic $\tilde{p}$.

$$p(\mathbf{r},t) = p_0(t) - \rho_0(t) g z + \tilde{p}(\mathbf{r},t) \tag{12}$$

where z is the vertical spatial component. After subtracting off the hydrostatic pressure gradient from Equation 2 and then dividing by the density, the equation becomes

$$\frac{\partial u}{\partial t} + \frac{1}{2}\nabla|u|^2 - u\times\omega + \frac{1}{\rho}\nabla\tilde{p} - \frac{\rho-\rho_0}{\rho}g = \frac{1}{\rho}(\nabla\cdot\sigma). \tag{13}$$

To simplify this equation further, the density in the pressure term is assumed ambient, and then the term $|u|^2/2$ is combined with the perturbation pressure $\tilde{p}/\rho_0$ and written as a total pressure, $\mathcal{H}$. This approximation assumes that the buoyancy-generated part of the vorticity field is much larger than the baroclinic part that is generated by the nonalignment of perturbation pressure and density gradients. This is not a good approximation at the small scales where the actual combustion heat release takes place. However, at the resolvable scales, this is nothing more than the assumption that these are buoyancy-dominated flows. The reason for neglecting the baroclinic term is so that a Poisson equation can be solved for the total pressure.

The treatment of subgrid scale mixing follows very closely the analysis of Smagorinsky (1963). The stress tensor σ in Equation 13 is replaced by the Reynolds stress tensor τ whose components are written in the form

$$\tau_{ij} = 2\rho(C_s\Delta)^2|S_{ij}|S_{ij} \quad ; \quad S_{ij} = \frac{1}{2}\left(\frac{\partial u_i}{\partial x_j} + \frac{\partial u_j}{\partial x_i}\right)$$

where C_s is taken as 0.21, $\Delta = (\delta x\, \delta y\, \delta z)^{\frac{1}{3}}$, and

$$|S_{ij}| = \sqrt{2\, S_{ij} S_{ij}}\,.$$

There have been numerous refinements of the original Smagorinsky model (Deardorff 1972; Germano et al. 1991; Lilly 1992), but it is difficult to assess the improvements offered by these newer schemes. There are two reasons for this. First, the structure of the fire plume is so dominated by the large-scale, resolvable eddies that even a constant eddy viscosity gives results almost identical with those obtained here (Baum et al. 1996). Second, the lack of precision in most large-scale fire data makes it difficult to sort out the subtleties associated with these models. For the time being, the Smagorinsky model with the given C_s produces satisfactory results for most large-scale applications where boundary layers are not important.

The fire itself is represented by introducing a large number of Lagrangian elements that release heat as they are convected about by the thermally induced motion. Since the fluid motion determines where the heat is actually released, and the heat release determines the motion, the large-scale features of the coupling between the fire and the smoke transport are retained. It should be noted, however, that the heat release rate is not predicted but is an input parameter in the computer programs implementing this model. The smoke is simulated by tracking the convected elements after the fuel burnout is completed. A fraction of the fuel consumed is assumed to be converted to smoke particulate. (The fraction of the fuel that is converted to smoke particulate, sometimes called the "smoke yield," is obtained from measurements of CO_2, CO, and particulate in a sample of the smoke. It is assumed that the carbon in the fuel ultimately is converted to one of these three products; thus, the ratio of particulate to the gases can be used to determine the smoke yield.) Thus, a knowledge of the spatial distribution of the Lagrangian elements is equivalent to a specification of the smoke particulate density at any instant of time. This thermal element model, which represents the combustion heat release as a large number of point sources convected by the resolvable flow field, is, in fact, a simple combustion model in its own right. It is consistent with more detailed combustion theories currently in use, and it permits the use of experimental data from fire experiments in a way that does not violate the consequences of those theories. A more detailed discussion of this model can be found in Baum et al. (1996).

Convective heat transfer to walls is accounted for by assuming a free convection heat transfer coefficient of the form

$$h = C(\Delta T)^{\frac{1}{3}} \tag{14}$$

where the constant C varies depending on the orientation of the surface. In special cases, where the computational grid is sufficiently resolved in the neighborhood of a wall, the convective heat transfer can be computed directly. However, for most practical applications, the empirical expression for heat transfer is used.

In summary, the equations that are solved numerically are the energy equation (11), the momentum equation (13), and a Poisson equation for the total pressure, obtained by taking the divergence of Equation 13. This linear elliptic equation is solved with the use of an FFT-based direct solver. The background pressure, temperature, and density are found from Equations 6, 7, and 10. Each of the conservation equations emphasizes the importance of the divergence and vorticity fields, as well as the close relationship between the thermally expandable fluid equations (Rehm and Baum 1978) and the Boussinesq equations for which the authors have developed highly efficient solution procedures (McGrattan et al. 1994; Baum et al. 1994). These are applied directly to the equations presented here with minor modifications and no loss in performance. The only changes from earlier methodology are a return to a uniform rectangular grid with blocks of cells masked to simulate internal boundaries and the use of a second order Runge-Kutta scheme to advance the velocity and temperature fields in time. The speed and accuracy of this technique enable calculations on current generation workstations that involve more than a million computational cells, yielding the spatial range of two orders of magnitude for a three-dimensional calculation.

ISOLATED FIRE PLUME

The most obvious test of the numerical model is to compute a buoyant plume from a fire. The fire plume is the single most important object of study in fire science. It provides the radiant energy source that generates the gasified fuel from the condensed phase needed to sustain the fire. It

also serves as the heat pump that both entrains air into the active combustion zone and then circulates the combustion products through the surrounding enclosure. It is the latter role that is of interest here. Although the central role of the fire plume has been recognized for some time, there is still much uncertainty about the plume structure. Indeed, Zukoski (1994) gives a recent summary of the state of knowledge of mass entrainment into isolated fire plumes. There is clearly no consensus on any simple formula or graphical correlation for this most basic of plume quantities. Much of this uncertainty arises from the experimental and conceptual difficulty associated with determining the outer plume boundary. McCaffrey (1979) developed centerline mean velocity and temperature correlations that are consistent with a large body of experimental data (Baum and McCaffrey 1989).

To perform a computational study of an isolated fire plume, the minimum length scale that must be resolved is the plume structure scale.

$$D^* = (Q/\rho_0 c_p T_0 \sqrt{g})^{2/5} \tag{15}$$

D^* is roughly comparable to the plume diameter near the base. It involves the heat release rate Q directly and can be seen both in the dimensionless form of McCaffrey's plume correlations and by considering the dimensionless form of the Navier-Stokes equations for this problem. In fact, if the equations discussed above are made nondimensional with D^* as length scale, $\sqrt{gD^*}$ as velocity scale, $\sqrt{(D^*/g)}$ as time scale, and T_0 as temperature, all the physical constants disappear from the inviscid terms in the equations. Only Reynolds and Prandtl numbers appear in the viscous stress and heat conduction terms.

In order to simulate the convective mixing of the fire plume, the grid spacing should be about 0.1 D^* or less. Figure 1 shows an instantaneous snapshot of three temperature contours obtained from a 96 × 96 × 96 cell simulation. The contours correspond to the boundaries of the continuous flame, intermittent flame, and plume zones as defined by Baum and McCaffrey (1989). Note that the image is an instantaneous snapshot of the fire and that time averages of the output of this kind of simulation must be produced in order to make quantitative comparison with most experimental data. Indeed, it is the fact that the results of the simulation can be averaged in a routine way while the equations of fluid mechanics cannot that is the basis of the whole approach presented here.

On the left of Figure 2 are the instantaneous vertical centerline velocity and temperature profiles superimposed on the steady-state correlation of McCaffrey (circles). The oscillations are primarily due to the large toroidal vortices generated at regular intervals at the base of the fire, which then rise asymmetrically. Note that the flow is not even remotely axially symmetric and the centerline is defined only by the geometry of the pool at the base of the plume. The right side of Figure 2 shows the corresponding time-averaged quantities (solid lines) and McCaffrey's centerline correlations. The time-averaged flow is symmetric and in excellent agreement with the correlations. The major deviations are at the bottom of the plume, where the thermal elements are turned on instantaneously without any preheat as they leave the pool surface. Otherwise, the boundaries of the computational domain are open. At these open boundaries, the perturbation pressure is assumed zero. This is a reasonable approximation at the side boundaries but less so at the top. Various strategies have been explored to properly set the conditions at the top, but in most instances, there is usually a solid ceiling or a hood drawing the combustion products up at some specified flow rate. Figure 3 shows the corresponding radial dependence of the vertical velocity and temperature at heights of $z/D^* = 2.8$ (intermittent region) and $z/D^* = 5.3$ (plume region). The results of the simulation are compared with Gaussian profiles that incorporate the half-widths obtained from McCaffrey's correlations.

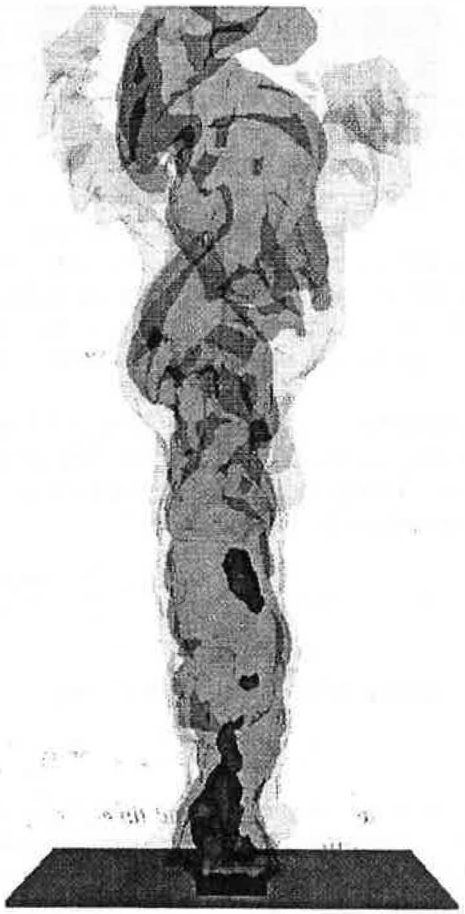

Figure 1 *Instantaneous snapshot of a pool fire simulation performed on a 96 × 96 × 96 grid. The contours correspond roughly to the boundaries of the continuous flame, intermittent region, and plume. The square burner is of length D* with the height of the computational domain rising to about 12 D*.*

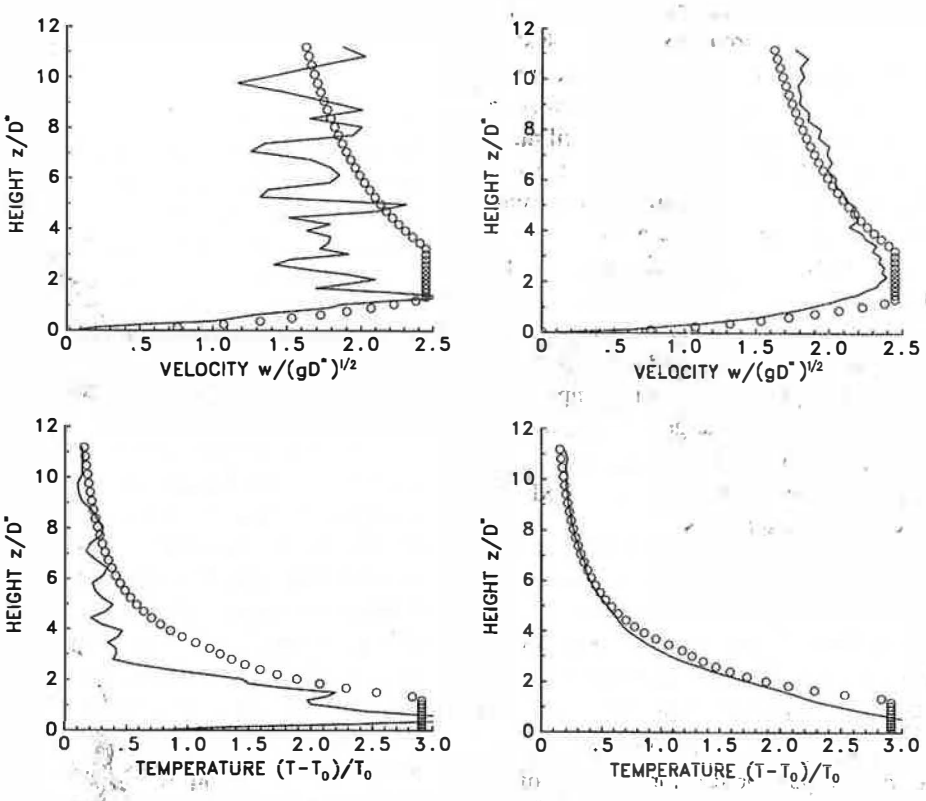

Figure 2 *Instantaneous (left) and time-averaged (right) centerline velocity and temperature profiles for the pool fire simulation shown in Figure 1.*

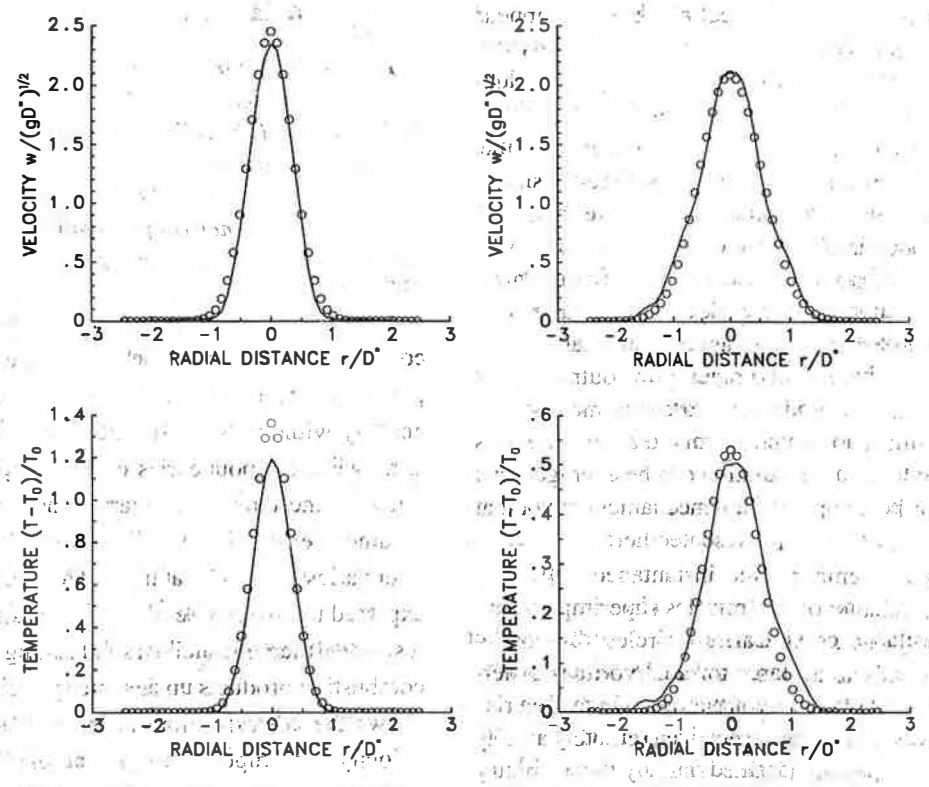

Figure 3 *Time-averaged radial profiles of vertical velocity and temperature at two vertical locations above the base of the simulated pool fire shown in Figure 1. On the left is the vertical location z/D* = 2.8 (intermittent region) and on the right is the vertical location z/D* = 5.3 (plume region).*

APPLICATIONS

There has been an ongoing debate in the fire protection engineering community as to the interaction between a sprinkler system and roof vents and draft curtains. This has led to a renewed effort by the National Fire Protection Association's Research Foundation and a group of interested industrial sponsors to conduct large-scale experiments of fires in a warehouse setting. In 1997, heptane spray burner and racked commodity fire experiments were conducted at the Large Fire Test Facility at Underwriters Laboratories in Northbrook, Illinois. The results of both the heptane spray burner and the commodity fires will be released in the spring of 1998. The purpose of this paper is not to describe these results in detail but rather to demonstrate how the numerical model was used in the analysis of the experiments.

The main test area in the new UL fire test facility consists of a 120 ft by 120 ft by 50 ft high enclosure, exhausted from above by a 60,000 cfm smoke duct and replenished by four makeup air ducts at floor level. Within this space is a 100 ft by 100 ft movable ceiling in which 4 ft by 8 ft vents were installed among a permanent array of sprinklers, spaced 10 ft apart on a rectangular grid. The flow rate from each sprinkler was set to 50 gpm. The ceiling was raised to a height of 25 ft and instrumented with 0.0625 in. diameter inconel sheathed type K thermocouples at each sprinkler location, thermocouple trees at each fire location, and thermocouples and pressure transducers above and below the vents. The ceiling was constructed of 2 ft by 4 ft by 5/8 in. thick fire-rated ceiling tiles. Draft curtains 6 ft deep were installed for some of the tests, enclosing areas of about 5,000 ft^2. The curtains were made of 18 gauge sheet metal.

The advantage of performing heptane spray burner experiments is that they are relatively inexpensive and well controlled. The heptane spray burner consisted of a 40 in. by 40 in. square of 0.5 in. pipe supported by cinder blocks. The heptane was ejected through atomizing spray nozzles distributed around the square, and the heat release rate from the resulting fire could be increased to about 10 MW. In all, 34 experiments were conducted with heptane burners. The results of these experiments were used to investigate the performance of the various fire protection systems and also to check the predictive capability of the numerical model because the heat release rate was well characterized.

The most obvious check of the numerical model is how well it predicts sprinkler activation times. Actually, the solution of the fluid equations only predicts the temperature and velocity of the hot gases near the sprinkler at any given time. In reality, activation is achieved when a small heat-sensitive link reaches a certain threshold temperature and releases the water. The solid phase conduction is not modeled directly but rather by solving a simple equation for the link temperature. The link temperature is estimated from the differential equation presented by Heskestad and Bill (1987),

$$\frac{dT_l}{dt} = \frac{\sqrt{u}}{RTI}(T_g - T_l) - \frac{C}{RTI}(T_l - T_m), \qquad (16)$$

where T_l is the link temperature, T_g is the gas temperature in the neighborhood of the link, T_m is the temperature of the sprinkler amount, and u is the gas velocity. The thermal sensitivity of the detector is indicated by the value of the Response Time Index, or RTI. The heat lost to the mount due to conduction is characterized by the C-Factor, C. A small wind tunnel or plunge oven is used to determine both of these parameters by creating an environment in which the air velocity and temperature, plus the mount temperature, are held at constant values.

Calculations were performed to predict the outcomes of the heptane spray burner tests. Depending on how much of the test space was simulated, the calculations required grids ranging from several hundred thousand to about a million computational elements. Typically, the area beneath the movable ceiling was modeled. The side boundaries of the domain were thus open, and it was assumed that the pressure there was ambient. The CPU time required to advance a one million cell simulation one time step is about 10 seconds on an RISC/6000 workstation. Typically, a time step is about one thirtieth of a second. Figure 4 presents a typical result from one of the tests, in which the sprinkler activation times from the experiment are compared with those from the numerical model. A more detailed comparison can be found in Figure 5, where the gas temperatures near the sprinklers are presented. In all of the calculations, the numerical model predicted the activation of the first four sprinklers surrounding the fire to within about 5 or 10 seconds. For the next row of sprinklers, the model tended to underpredict the activation times by 15 to 30 seconds, on average. This difference probably is due to the uncertainty in the droplet size distribution. The calculations were performed assuming an average droplet diameter of 2 mm. The smaller droplets that are responsible for much of the cooling may not have been accounted for. Numerical runs were performed with both overestimates and underestimates of droplet sizes, and the temperatures downstream of activated sprinklers changed significantly. The true answer lies somewhere in between, and efforts are still being made to more accurately measure the droplet sizes. The thermocouple data, compared with the numerical data, points out just how sensitive the activation times are to temperature changes of just 5 or 10 degrees.

In addition to the heptane spray burner experiments, five experiments were performed in which racks of cartoned plastic cups were burned in the same test area as the heptane fires. A standard plastic test commodity served as the fuel for these tests. The plastic commodity consists of rigid crystalline polystyrene jars (empty, 16-oz. size) packaged in compartmented, single-wall, corrugated paper cartons. Jars are arranged in five layers, 25 per layer, for a total of 125 per carton. Eight 21 in. cube cartons, arranged 2 × 2 × 2, compose a pallet load. Two-way, 42 in. × 42 in. × 5 in. slatted deck hardwood pallets support the loads. A pallet load weighs approximately 170 lb,

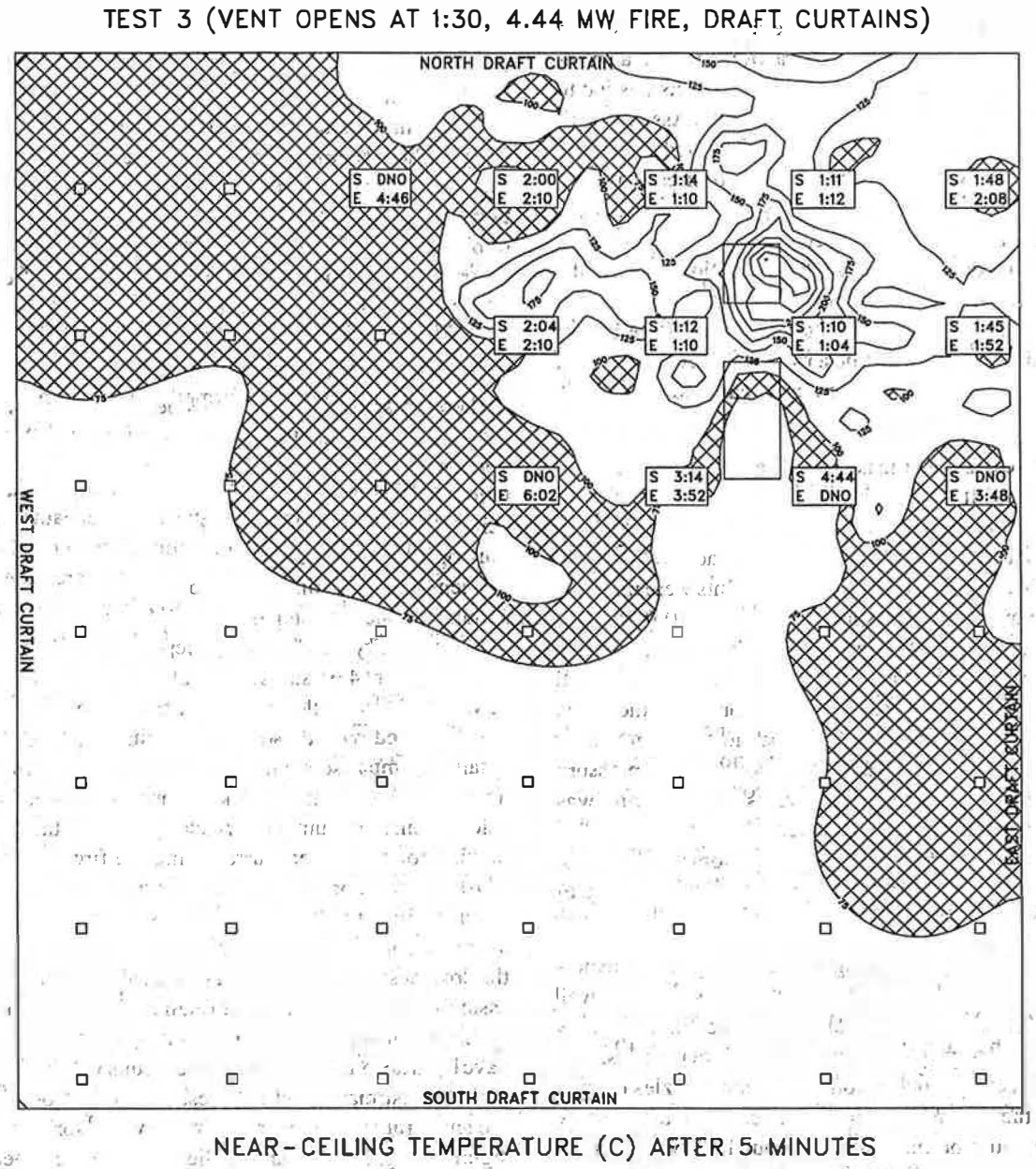

Figure 4 *Sprinkler activation times for one of the heptane spray burner experiments (E) and the corresponding numerical simulation (S). The temperature contours were calculated by the numerical model. The cross-hatched area represents temperatures in the range of 75°C to 100°C. The sprinklers are designed to activate at a temperature of 74°C, but due to conductive losses to the mount, they usually activate when the smoke temperature rises above 100°C.*

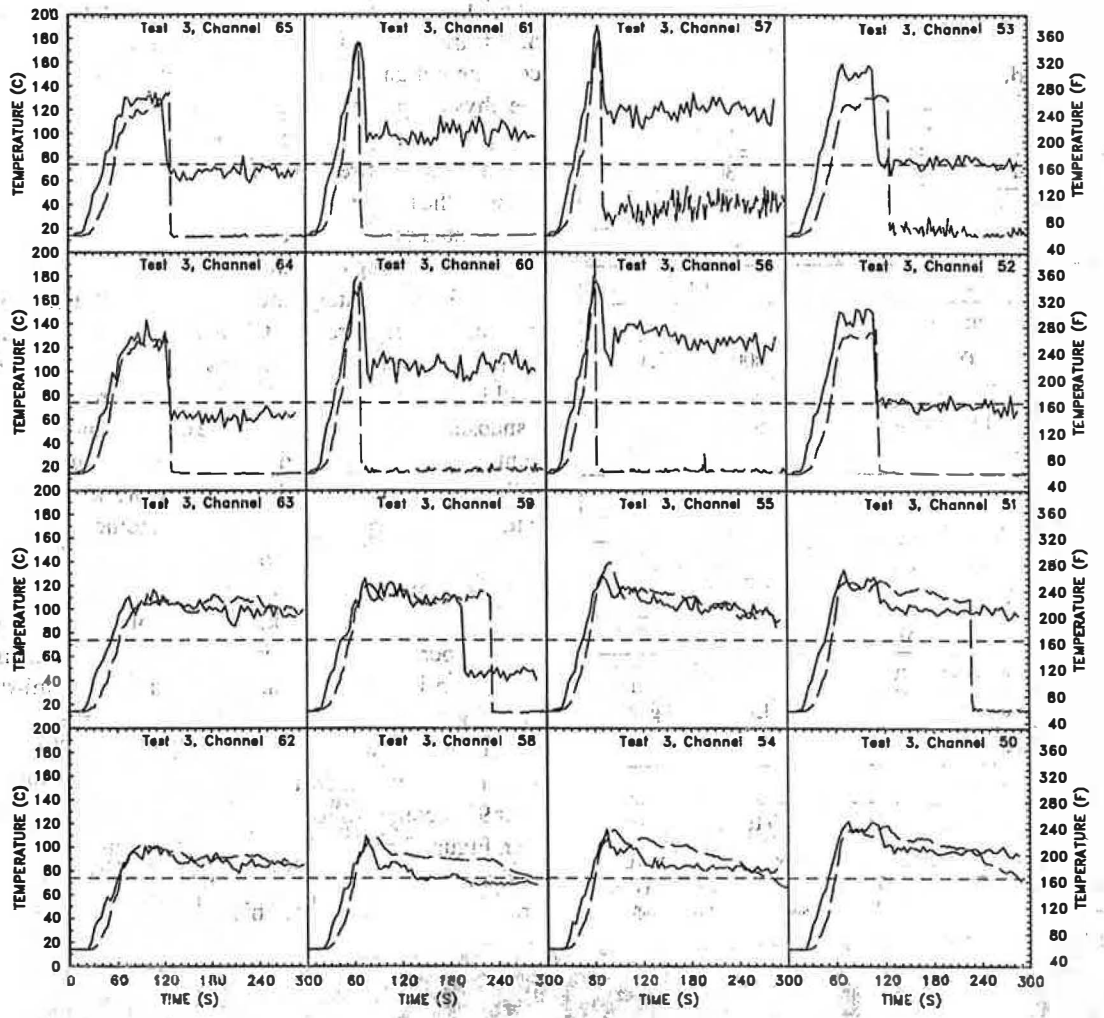

Figure 5 *Comparison of experimental (dashed curve) and simulated (solid curve) temperatures of the near-sprinkler thermocouples for the sample heptane spray burner experiment. The activation temperature of the sprinkler (74°C, 165°F) is denoted with a short dashed line. The channel numbers refer to the four-by-four array of sprinklers in the upper right-hand corner of Figure 4. Note that when the experimental temperature (dashed curve) suddenly drops back to ambient, the sprinkler has activated and the thermocouple can no longer be used to measure the smoke temperature.*

of which about 36% is plastic, 35% is wood, and 29% is corrugated paper (Troup 1994). The rack configuration was designed to replicate typical storage situations found in warehouse-type retail stores. Each storage array consisted of a main (ignition) double-row rack at the center, flanked on two sides by two single-row targets. The rows were separated by 8 ft wide aisles. The main double-row racks each consisted of four 8 ft long bays; a 6 in. flue separated the rows. Longitudinal flues of 8 in. were used to separate the pallets within a row. The overall loaded area of the double-row rack measured approximately 7.5 ft wide × 33 ft long. The racks were divided vertically into four tiers; the overall loaded height was 19 ft. A similar configuration was used in a series of burns documented by Troup (1994).

Simulations of the plastic commodity experiments are much more difficult to perform because of the inclusion of complex phenomena governing the fire growth, flame spread, sprinkler spray dynamics, and extinguishment. Table 1 lists some of the input parameters required by the numerical code to perform a simulation. Most of these values were measured in bench scale experiments. Wherever possible, the numerical model makes use of information or measurements that can be easily obtained from small-scale experiments. The intent of the modeling is not to predict everything from first principles but rather to combine the results of tractable experiments to predict the results of experiments that are difficult and costly to perform.

In addition to the input parameters listed in Table 1, the numerical algorithm contains logic that dictates how water

TABLE 1
Required Input Parameters for an Industrial Fire Simulation*

Category	Parameter	Value
Geometry	Overall Dimensions	30.5 m × 30.5 m × 8.2 m
	Boxes/Pallet Dimensions	1.1 m × 1.1 m × 1.2 m
Numerical	Grid Dimensions	144 × 144 × 40
	Cell Size	0.21 m × 0.21 m × 0.21 m
Fuel	Ignition Temperature	370°C
	Lumped Thermal Capacitance	1000 J/(m^2·K)
	Heat Release Rate Per Unit Area	500 kW/m^2
	Energy Content Per Unit Volume	500 MJ/m^3
	Radiative Fraction	0.45
Sprinkler	Response Time Index (RTI)	114 (m·s)$^{1/2}$
	C-Factor (Eq. 16)	0.8 (m/s)$^{1/2}$
	Activation Temperature	74°C
	Flow Rate	189 L/min. (50 gpm)
	Spray Angle	5° - 80°
	Initial Droplet Velocity	8 m/s
	Droplet Diameter Range	100 μm - 2000 μm
	Sprinkler Spacing	3 m × 3 m (10 ft × 10 ft)

*Note that the term "lumped thermal capacitance" is used to denote the product of the density, specific heat, and thickness of cardboard boxes containing the plastic cups.

droplets will behave when they encounter an obstacle, how heat is transferred from the water to the fuel, how the droplets cool the hot gases, and so on. A detailed description of all of the physical processes that are modeled is beyond the scope of this paper. At issue here is how the numerical model can be used to analyze fire experiments. An interesting case to examine with the numerical model was an experiment where the fire was ignited directly beneath a vent, but the vent failed to open due to the wetting of its automatic fusing mechanism. What if it had? Unfortunately, there was not enough money in the project budget to repeat the test. Instead, a calculation was performed where the vent was allowed to open when its fusible link reached its design temperature. Figure 6 presents a snapshot of the simulation. The calculation predicted that the vent should have opened 92 seconds after ignition of the fire, followed a second later by the first sprinkler and 20 seconds later by the second sprinkler. Another calculation was performed in which the vent was assumed to open 40 seconds after ignition. This case was intended to address the strategy of opening vents as quickly as possible by means of either a low-temperature fusible link or smoke detector. In this case, the first sprinkler did not activate until 2:09. A third version of the experiment was simulated in which the vent was held closed, which was, in fact, the unanticipated result of the actual experiment. In this case, the first sprinkler activated after 93 seconds, followed 2 seconds later by the second sprinkler. Figure 7 presents the heat release rate for the simulations of the three versions of the experiment. Given the very rapid growth of the fire during this period, it is no surprise that the

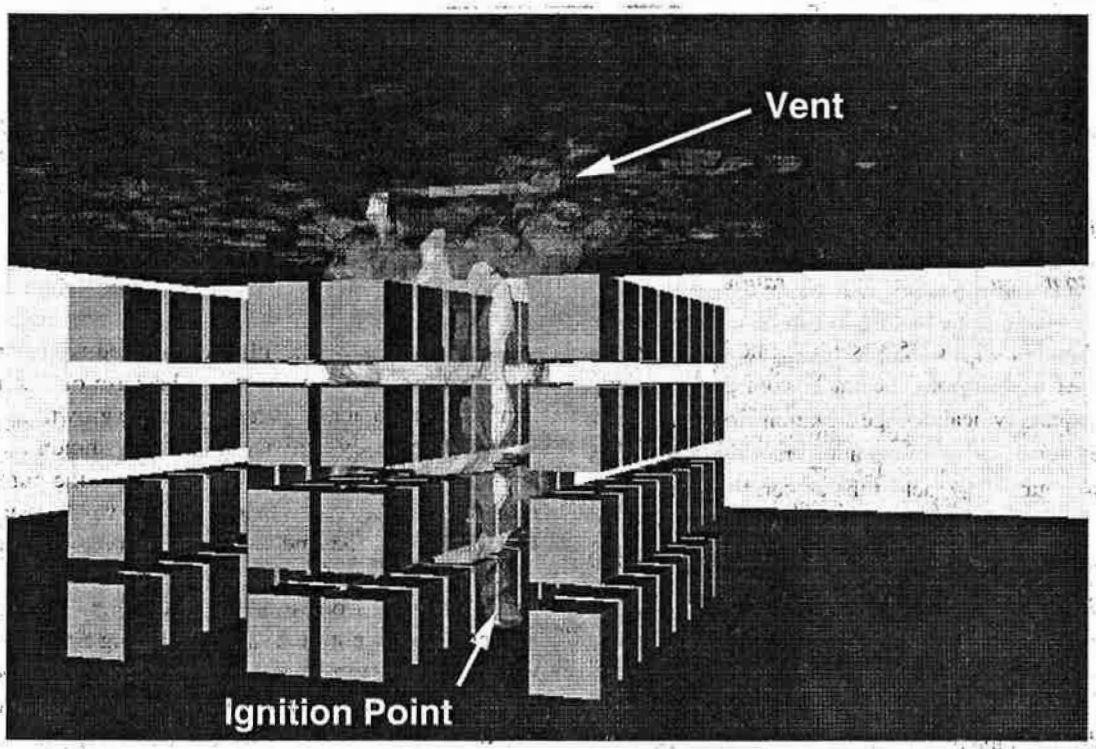

Figure 6 Numerical simulation of a plastic commodity fire experiment.

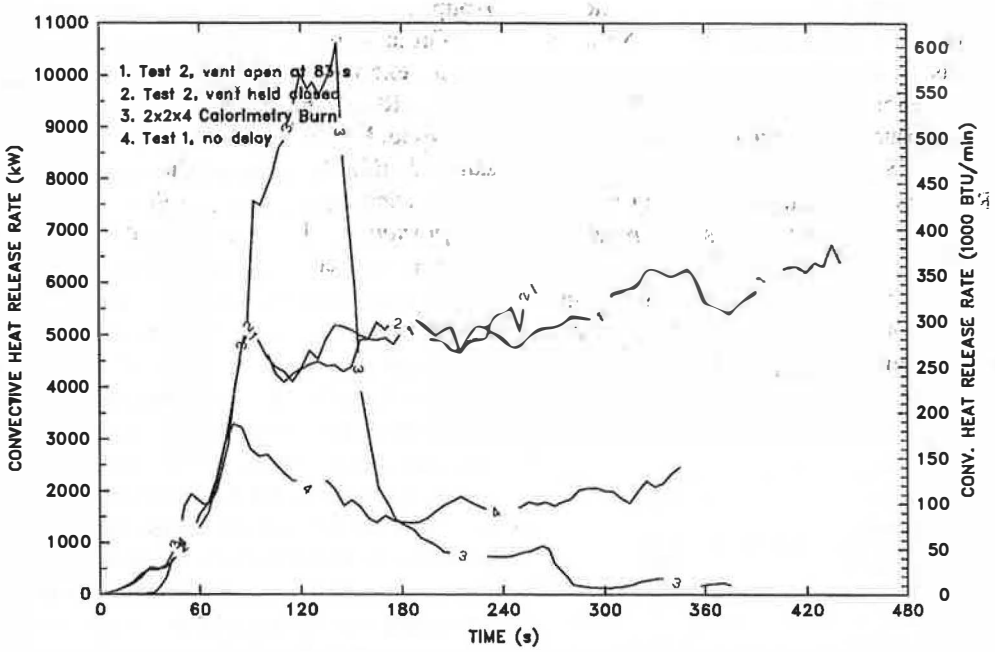

Figure 7 *Heat release rates for three similar simulations of a plastic commodity fire experiment in which the ignition location is directly beneath a roof vent. The curves represent scenarios where the vent is opened manually 40 seconds after ignition, automatically 92 seconds after ignition, and not opened at all.*

heat release rate grows to about 7 MW in the case where the vent is opened early. The case where the vent opened automatically at 92 seconds shows a higher heat release rate than the case where the vent was held closed. This is due to the fact that the second sprinkler in the former case was delayed 20 seconds by the opening of the vent.

CONCLUSION

These examples illustrate the usefulness of the numerical model. The types of fire experiments described can cost tens of thousands of dollars each. Given the range of parameters that need to be examined in a given test series, the numerical model can provide a very cost-efficient means of simulating experiments. Although modeling will probably never eliminate the need for large-scale testing, it can be used to reduce its cost by expanding on the limited results obtained from a small number of experiments. Using computations to plan experiments decreases the number of tests necessary because they can isolate those configurations that best demonstrate the effectiveness of a particular method or device. As a post-experiment analytical tool, the simulations can be used to distinguish the various phenomena at work in a given fire scenario. The numerical model is particularly useful in this regard because it eliminates much of the variability that is seen in real fire experiments. When two calculations are performed in which only one parameter is changed, the difference in outcomes can safely be attributed to that parameter. However, when two large-scale fire tests are performed with the same parameter changed, it is never certain that the difference in results can be attributed to that parameter. Usually, a number of replicate tests need to be performed, driving the cost of testing still higher.

REFERENCES

Baum, H.R., and B.J. McCaffrey. 1989. Fire induced flow field—Theory and experiment. *Fire Safety Science—Proceedings of the Second International Symposium*, pp. 129-148. New York: Hemisphere.

Baum, H.R., O.A. Ezekoye, K.B. McGrattan, and R.G. Rehm. 1994. Mathematical modeling and computer simulation of fire phenomena. *Theoretical and computational fluid dynamics*, Vol. 6, pp. 125-139.

Baum, H.R., K.B. McGrattan, and R.G. Rehm. 1996. Three dimensional simulations of fire plume dynamics. *Journal of the Heat Transfer Society of Japan*, Vol. 35, pp. 45-52.

Deardorff, J.W. 1972. Numerical investigation of neutral and unstable planetary boundary layers. *Journal of Atmospheric Sciences*, Vol. 29, pp. 91-115.

Germano, M., U. Piomelli, P. Moin, and W.H. Cabot. 1991. A dynamic subgrid-scale eddy viscosity model. *Physics of Fluids A*, Vol. 3, pp. 1760-1765.

Heskestad, G., and R.G. Bill. 1987. Conduction heat loss effects on thermal response of automatic sprinklers. Factory Mutual Research Corporation.

Lilly, D.K. 1992. A proposed modification of the Germano subgrid-scale closure method. *Physics of Fluids A*, Vol. 4, pp. 633-635.

McCaffrey, B.J. 1979. Purely buoyant diffusion flames—Some experimental results. NBSIR 79-1910, National Bureau of Standards.

McGrattan, K.B., R.G. Rehm, and H.R. Baum. 1994. Fire-driven flows in enclosures. *Journal of Computational Physics*, Vol. 110, pp. 285-291.

Rehm, R.G. and H.R. Baum. 1978. The equations of motion for thermally driven, buoyant flows. *Journal of Research of the NBS*, Vol. 83, pp. 297-308.

Smagorinsky, J. 1963. General circulation experiments with the primitive equations. I. The basic experiment. *Monthly Weather Review*, Vol. 91, pp. 99-164.

Troup, J.M.A. 1994. Large-scale fire tests of rack stored Group A plastics in retail operation scenarios protected by extra large orifice ({ELO}) sprinklers. Report J.I. 0X1R0.RR, Factory Mutual Research Corporation, Norwood, Mass.

Zukoski, E.E. 1994. Mass flux in fire plumes. *Fire Safety Science—Proceedings of the Fourth International Symposium*, pp. 137-148. International Association for Fire Safety Science.